Agricultural land-use composition modulates hydroclimatic coupling of cropland water use efficiency under prolonged aridification: sub-watershed evidence from Chile's megadrought

(This paper is a non-peer reviewed preprint submitted to EarthArXiv)

Francisco Zambrano[a,*], Francisco Fernández[b], María Molinos-Senante[c]

[a] *Facultad de Medicina Veterinaría y Agronomía, Universidad de Las Américas, Chile,*

[b] *Facultad de Economía, Negocios y Gobierno, Universidad San Sebastián, Santiago, Chile,*

[c] *Institute of Sustainable Processes, Universidad de Valladolid, Valladolid, Spain, 47011*

Abstract

Cropland water-use-efficiency (WUE; operationalized as net primary productivity divided by actual evapotranspiration) is widely expected to improve under technological intensification, yet its response to prolonged aridification at regional scales is poorly understood. We analyzed spatiotemporal patterns of WUE across 127 Chilean agricultural sub-watersheds from 2001 to 2020, a period spanning an unprecedented megadrought. WUE responses were spatially heterogeneous, arid and semi-arid sub-watersheds showed predominantly negative ΔWUE, while irrigated Mediterranean sub-watersheds showed positive ΔWUE; negative long-term trends and structural breaks concentrated in the 30-35°S band. Precipitation deficit indices dominated cross-sectional WUE sensitivity; at the 36-month accumulation scale, SPEI (Standardized Precipitation-Evapotranspiration Index) and SPI (Standardized Precipitation Index) showed practically equivalent explanatory power (two one-sided test $p < 0.001$, 90% CI $[-0.004, +0.003]$). Crop system composition is associated with WUE drought sensitivity through two contrasting patterns, each constrained by a different form of confounding. Annual-crop prevalence is robustly and negatively associated with drought sensitivity across all latitude specifications (spatial error model [SEM] $\beta = -0.322$ to -0.485, $p < 0.01$); whether this reflects structural buffering or drought-driven reduction of annual cultivation cannot be established from the observational data alone. Irrigation infrastructure prevalence is positively associated with WUE-drought coupling in the full sample (SEM $\beta = +0.422$, $p < 0.001$), but this association attenuates to non-significance when latitude is explicitly controlled ($\beta = +0.109$, $p = 0.327$) and cannot be statistically isolated from the latitudinal aridity gradient; within the warm-summer-Mediterranean zone the association is marginal ($\beta = +0.264$, $p = 0.053$). Both patterns are associative; causal inference is not possible given the observational design and spatial confounding. These patterns are consistent with crop-portfolio flexibility reducing structural drought exposure under prolonged aridification, and with WUE-based efficiency metrics being insufficient indicators of agricultural resilience where irrigation supply is hydrologically coupled to the same signals that suppress crop productivity. These findings have implications for water governance and agricultural planning in snowmelt-dependent dryland regions globally.

Keywords: water use efficiency, megadrought, aridification, SPEI, Chile, NPP/ET, crop composition

1. Introduction

Global agriculture consumes approximately 70% of freshwater withdrawals (Hoekstra and Mekonnen, 2012), yet whether irrigation infrastructure buffers or amplifies cropland ecosystem water use efficiency (WUE; NPP/ET) sensitivity under prolonged drought remains poorly understood. The widely held assumption that irrigation protects crop production from meteorological variability has been challenged on two fronts. The irrigation efficiency paradox shows that technical efficiency gains can paradoxically increase aggregate water consumption by enabling crop intensification (Grafton et al., 2018; Ward and Pulido-Velázquez, 2008). Demand-hardening dynamics predict that structural commitment to irrigation infrastructure creates inelastic water demand that amplifies drought vulnerability when supply fails, while annual crop flexibility provides only partial adjustment capacity (Grafton et al., 2018). Whether these mechanisms operate at the watershed scale under a multi-year megadrought remains poorly established. As aridification intensifies across dryland and Mediterranean-climate regions (Gebrechorkos et al., 2025; Zambrano et al., 2025), whether managed irrigation systems buffer or transmit hydroclimatic stress is a critical question for adaptive water governance (FAO y ONU Agua, 2025; Howden et al., 2007; Wallace, 2000). Chile's central Mediterranean zone, where irrigated perennial agriculture draws on Andean snowmelt-fed rivers under a decade-long megadrought (Boisier et al., 2018; Garreaud et al., 2020), provides a natural experiment at the intersection of these questions.

Cropland ecosystem WUE drought sensitivity at the regional scale has received growing attention, yet critical empirical gaps limit predictive understanding. Most analyses of WUE variability under drought focus on global or continental means, obscuring the sub-watershed scale heterogeneity that governs local management relevance (Ito and Inatomi, 2012; Yu et al., 2025). Studies comparing irrigated and rainfed

*Corresponding author
Email addresses: fzambrano@udla.cl (Francisco Zambrano), francisco.fernandez@uss.cl (Francisco Fernández), maria.molinos@uva.es (María Molinos-Senante)

systems have concentrated on yield or harvested-area adjustments rather than on the integrated net primary productivity (NPP) per evapotranspiration (ET) signal that ecosystem WUE captures, leaving unclear how irrigation infrastructure and crop type jointly modulate WUE drought sensitivity (Chakraborti et al., 2023; Davis et al., 2017). The distinct contributions of precipitation deficits versus atmospheric evaporative demand to WUE variability have rarely been quantified simultaneously across contrasting crop systems, so which aridification process drives WUE coupling most strongly remains an open question (AghaKouchak et al., 2015; Hobbins et al., 2016; Zambrano et al., 2025). Most critically, the demand-hardening prediction that structural irrigation infrastructure amplifies rather than buffers drought vulnerability has not been tested against observed WUE data across a sustained multi-year megadrought, where supply constraints accumulate rather than recover between seasons (Grafton et al., 2018; Tahasin et al., 2024; Ward and Pulido-Velázquez, 2008). Whether annual-crop portfolio flexibility provides structural buffering at the sub-watershed scale, independent of the latitudinal aridity gradient that co-varies with both irrigation prevalence and drought intensity, remains untested (FAO y ONU Agua, 2025; Howden et al., 2007).

This paper examines how agricultural crop system composition modulates WUE drought sensitivity across 127 Chilean sub-watersheds (2001–2020). Crop composition likely mediates the response to supply constraints: perennial fruit crops maintaining year-round root systems may sustain productivity under partial deficits, whereas annual crops allow area-based adjustment when supply falls critically short (Chakraborti et al., 2023; Davis et al., 2017). The analysis addresses two primary questions: (1) does annual-crop prevalence buffer WUE drought sensitivity independent of the latitudinal aridity gradient, and (2) is irrigation infrastructure prevalence associated with amplified sensitivity consistent with demand-hardening dynamics? Secondary questions address which aridification signal (Standardized Precipitation Evapostranspiration Index [SPEI], Standardized Precipitation Index [SPI], or (Evaporative Demand Drought Index, [EDDI]) most strongly predicts WUE variability and whether WUE responses are spatially clustered. Aridification is treated as multi-process using three complementary drought indices: SPEI (Vicente-Serrano et al., 2010) (hydroclimatic balance), SPI (Mckee et al., 1993) (precipitation deficit), and EDDI (AghaKouchak et al., 2015; Hobbins et al., 2016; McEvoy et al., 2016) (atmospheric evaporative demand). The primary analysis uses a spatial error model framework with 2021 post-drought census crop composition data. All findings are associative; causal inference is not possible given the cross-sectional observational design and spatial confounding.

2. Data and Methods

2.1. Study area

Continental Chile (approximately 17°S to 56°S) spans extreme latitudinal climate gradients, from the hyperarid Atacama in the north to the Mediterranean zone (32°S–38°S) concentrating the majority of irrigated agriculture, viticulture, and fruit export production, and a humid-temperate zone supporting rainfed cereals and forages south of 38°S (Figure 1). The megadrought most severely affected the 30°S–42°S band, where precipitation deficits of 25–45% relative to the twentieth-century mean have persisted since 2010 (Boisier et al., 2018; Garreaud et al., 2020). The study uses sub-watershed-level spatial units based on Chilean National Water Authority (DGA) hydrological boundaries, which align with the country's water allocation governance framework (Rivera et al., 2016). Chile's 1981 Water Code established a privatized, market-based water governance system in which water rights are tradeable property and drought allocation is governed primarily by seniority and market exchange rather than state emergency intervention (Malagueño and D'Odorico, 2024).

2.2. WUE data

Annual cropland WUE ($\mathrm{g\,C\,kg^{-1}\,H_2O\,yr^{-1}}$), defined as $WUE = NPP/ET$, was obtained from the global cropland WUE dataset of Jiang et al. (2025), providing 1-km annual rasters for 2001–2020. This NPP/ET formulation represents the ecosystem WUE concept, which quantifies biophysical carbon-water coupling efficiency across the land surface, and is distinct from the agronomic WUE metric (crop yield per unit of water applied or consumed) used in irrigation management; both capture efficiency but over different process domains and at incompatible scales of observation. NPP was estimated using an Evaporative Fraction Light-Use Efficiency (EF-LUE) model driven by ERA5-Land reanalysis, GLASS fAPAR and LAI, and ESA CCI-LC land cover, calibrated against FLUXNET2015 flux towers across multiple climate zones. ET was obtained from the ETMonitor product (Hu and Jia, 2015), validated against flux towers ($r > 0.75$). WUE rasters were cropped to Chile's extent and annual mean WUE was extracted per sub-watershed by spatial averaging. The 20-year series (2001-2020) spans a pre-megadrought reference period (2001-2009) and the megadrought period (2010-2020). The WUE was standardized using z-scores for the years 2001-2020 and will be used in this context.

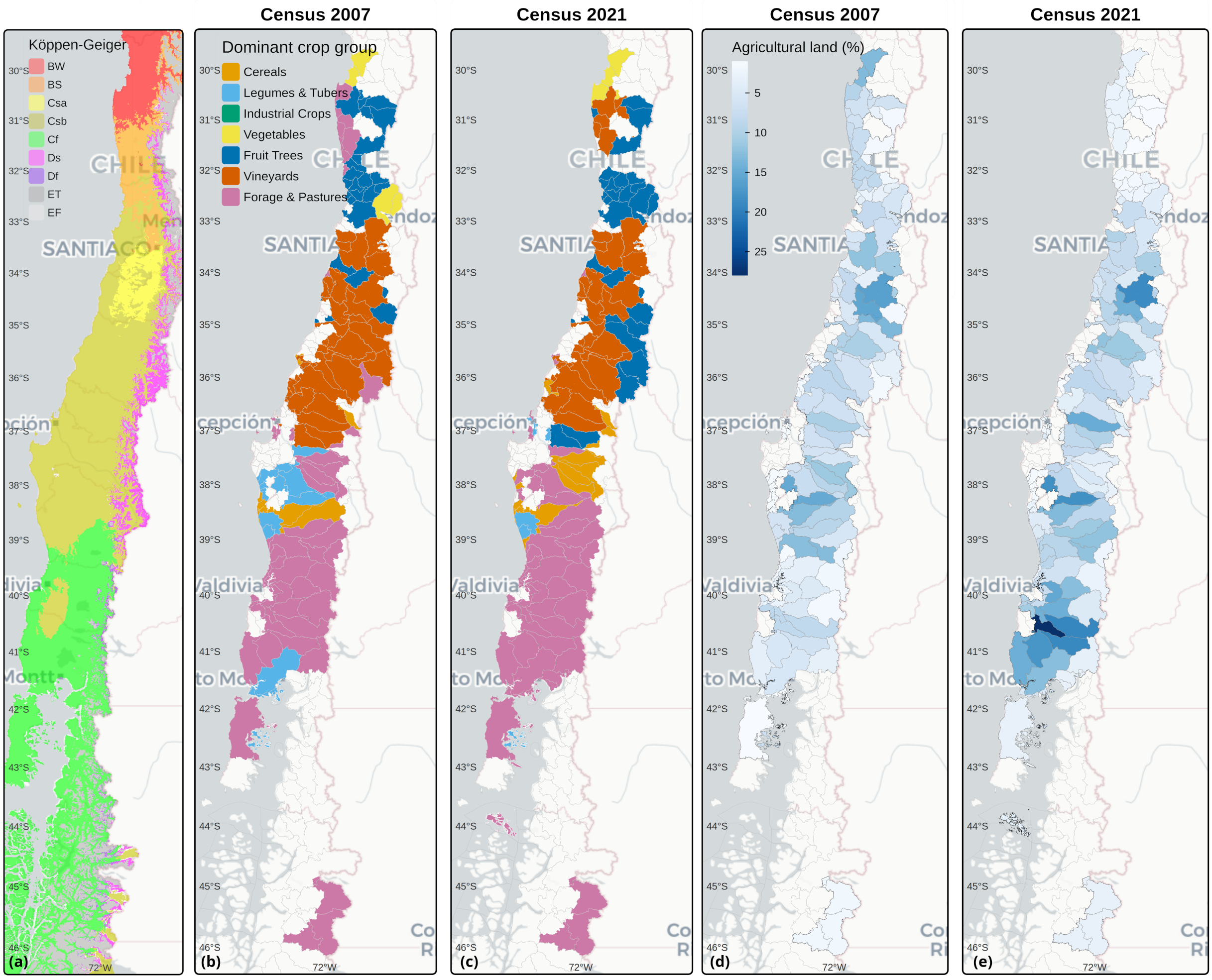

Figure 1: Study area and agricultural context across central Chile. (a) Köppen-Geiger climate classification across the study domain, spanning arid (BW) and semi-arid (BS) zones in the north, the warm- and hot-summer Mediterranean centre (Csa, Csb), and the humid-temperate south (Cf). (b-c) dominant agricultural crop group per sub-watershed, derived from the VII (2007) and VIII (2020-2021) Chilean Agricultural and Forestry Censuses. (d-e) agricultural land as a percentage of total sub-watershed area for the same two census years. Sub-watershed boundaries (DGA) are outlined in grey.

2.3. Drought drivers and WUE mechanistic components

2.3.1. Aridification drivers

Three complementary drought indices characterize distinct aridification dimensions (AghaKouchak et al., 2015; Zambrano et al., 2025). SPEI (primary driver) captures the hydroclimatic balance incorporating both precipitation and atmospheric evaporative demand (Vicente-Serrano et al., 2010). It was computed from CHIRPS (Climate Hazards Group InfraRed Precipitation with Station data) monthly precipitation (Funk et al., 2015) and FAO-56 Penman-Monteith reference evapotranspiration derived from CHIRTS-daily temperature data (Climate Hazards Center Infrared Temperature with Stations, (Funk et al., 2019)), then aggregated to a monthly basis. SPI isolates precipitation deficits from the same CHIRPS series (Mckee et al., 1993). EDDI characterizes anomalies in atmospheric evaporative demand independently of precipitation (Hobbins et al., 2016; McEvoy et al., 2016), computed from CHIRTS-based derived reference evapotranspiration. We used the EDDI sign convention to indicate that positive values represent below-normal evaporative demand, while negative values signify above-normal demand, thereby aligning EDDI with the polarity of SPEI and SPI. Each index was computed at 12, 24, and 36-month accumulation scales. The three indices were standardized via the empirical probability-weighted normal approximation. The December value for each year was retained as the annual index observation.

All three drought indices are derived from CHIRPS precipitation and CHIRTS temperature data, observation-based satellite-gauge merged products independent of the ERA5-Land reanalysis used by the EF-LUE model; the crop composition spatial error model uses relative cross-watershed sensitivity rankings unaffected by any spatially uniform forcing. Mean within-sub-watershed temporal R^2 at the per-family optimal scales was 0.277 for SPEI-12, 0.264 for SPI-12, and 0.168 for EDDI-24; SPEI-12 and SPI-12 show practically equivalent temporal explanatory power (TOST [Two One-Sided Tests] within ± 0.05 margin: $p < 0.001$, 90% confidence intervals [CI] [+0.007, +0.019]). Drought indices are standardized temporal anomalies relative to each sub-watershed's local historical mean and carry little information about the absolute spatial aridity gradient at any single time point; near-zero unique cross-sectional variance attributable to drought indices is a dimensional artefact of standardization, not evidence that drought matters less than crop composition for WUE. The SPEI–SPI cross-sectional equivalence result is reported in Section 3.4.

2.3.2. WUE mechanistic components

We used the NPP (MOD17A3HGF, MODIS Terra, 500 m, Collection 6.1), which was z-score standardized within 2001-2020 (zNPP), which will be called NPP hereafter; and SETI-12 (Paruelo et al., 2016) (Standardized

Evapotranspiration Index, 12-month scale; derived from MOD16A2GF actual evapotranspiration Running et al. (2021)). These are used exclusively as descriptive spatial context variables for the trend comparison in Section 3.1. The primary CASEarth WUE dataset does not distribute its internal NPP (EF-LUE model) and ET (ETMonitor) component layers separately, making algebraic decomposition infeasible. Because MOD17 and MOD16 have different sensitivities and error structures from the EF-LUE and ETMonitor models, NPP and SETI-12 are not used for formal component attribution of WUE variance, and no cross-product comparison of their relative sensitivities is presented.

2.4. Agricultural census data

Crop composition data were obtained from the VII Census (2007, pre-drought baseline) (INE, 2007) and the VIII Census (2020–2021, endpoint) (INE, 2021), both reporting cultivated area by crop category and management type at commune level. Commune-level data were spatially aggregated to sub-watershed level using area-weighted means. Three functional aggregates were computed for use as regression predictors: *pct_perennials* (fruit trees + vineyards), *pct_annuals* (cereals + vegetables + legumes + industrial crops), and *pct_forage* (forage/pasture; reference category). The variable *pct_irrigated* measures the census-reported proportion of agricultural land classified as irrigated, reflecting irrigation infrastructure and historical water rights, not the volume of water actually delivered in any given year. Sub-watersheds with high *pct_irrigated* have more irrigation-dependent cropping systems and greater structural exposure to supply disruptions. Dominant crop type per sub-watershed was assigned using a 40% area threshold.

The 2021 census irrigated area variable is derived entirely from directly reported data and underpins the primary spatial error model results. The 2007 irrigated area variable required partial imputation for six of ten crop categories using a commune-level residual ratio; because this single ratio is applied uniformly across categories with very different true irrigation intensities, it fundamentally distorts the cross-sectional variance structure of the 2007 pct_irrigated variable, and measurement error in this predictor spills over to bias the coefficients of correlated predictors in the same multiple regression. The 2007 model is therefore reported only in Supplementary Table S-9. Crucially, the imputation affects only the riego/secano split, not the total cultivated area per category, which is directly and completely reported in the VII Census for all ten crop groups. The 2007 baseline model therefore deliberately excludes pct_irrigated and relies exclusively on total area proportions. A sensitivity comparison adding the imputed irrigation predictor (Supplementary Table S-9) shows that the fruit-tree coefficient attenuates substantially from $= +0.732$ ($p < 0.001$) to $= +0.264$ ($p = 0.028$), consistent with measurement-error spillover from the imputed irrigation variable

(Frisch–Waugh–Lovell theorem).

2.5. Statistical analyses

Two sub-watershed sample sizes appear throughout the analyses n = 131 sub-watersheds have a complete 20-year WUE time series and are used for analyses requiring only the WUE series. The Pettitt change-point test and the two-way fixed-effects panel regression n = 127 sub-watersheds additionally satisfy two requirements: a valid prewhitened Mann-Kendall trend slope, and complete census-derived crop composition and irrigation data. This set is used for Mann-Kendall trend analysis, per-sub-watershed WUE-drought sensitivity slopes, and all crop composition regression models. The 127-sub-watershed set is a strict subset of the 131-sub-watershed set; the four sub-watersheds present in the larger set lack complete census or irrigation coverage and are excluded from composition analyses only. A full analytical inventory is provided in Supplementary Table S-1.

2.5.1. Trend and change-point analyses

Mann-Kendall trend tests and Sen's slope estimates (with prewhitening) were computed per sub-watershed for WUE, NPP, SETI-12, and EDDI-12 (2001-2020). The Pettitt test (Pettitt, 1979) was applied to each WUE series to detect the most probable year of mean-level shift. Benjamini-Hochberg (BH) false-discovery-rate (FDR) correction was applied across 131 simultaneous tests. Sub-watersheds were classified by significance ($p < 0.05$) and proximity to megadrought onset (break years within ± 2 years of 2010). A permutation null model (B = 1000 iterations per sub-watershed, seed = 2026) tested whether the observed break-year concentration near 2010 is distinguishable from a SPEI-step-change tracking null. Within-sub-watershed residuals from a SPEI-12 OLS (ordinary least squares) regression were resampled with replacement and the Pettitt test was re-run on each reconstructed null series. Observed and null break-year distributions were compared using a two-sample Kolmogorov-Smirnov (KS) test. Mean WUE was compared between the pre-megadrought (2001-2009) and megadrought (2010-2020) periods using Wilcoxon signed-rank tests, stratified by Köppen climate class.

2.5.2. WUE-aridification relationships

Spearman correlations and OLS sensitivity slopes ($\Delta WUE/\Delta Index$) were computed per sub-watershed across the 20-year series. Per-sub-watershed maps are treated as descriptive summaries given strong spatial autocorrelation (Moran's I = 0.509-0.683); confirmatory inference rests on the spatial error models and FDR-corrected Pettitt analysis. Moran's I and Getis-Ord Gi* local statistics identified spatial clustering and hotspots of WUE trend slope using queen contiguity weights. A two-way fixed-effects (TWFE) panel regression estimated:

$$WUE_{it} = \beta \cdot Index_{it} + \mu_i + \tau_t + \varepsilon_{it} \tag{1}$$

where μ_i and τ_t are sub-watershed and year fixed effects. Standard errors are Driscoll-Kraay (DK; Driscoll and Kraay (1998); bandwidth = 2), consistent for both serial correlation and cross-sectional spatial dependence. DK SEs (standard errors) inflate 3-4× relative to conventional HC1 (Heteroskedasticity-Consistent) clustered SEs, reflecting the strong spatial common component (full comparison in Supplementary Table S-11).

2.5.3. Crop composition and WUE sensitivity

The per-sub-watershed OLS slope of WUE regressed on SPEI-12 was used as the outcome in a multiple regression:

$$Sensitivity_i = \beta_0 + \beta_1 \cdot pct\_perennials_i + \beta_2 \cdot pct\_annuals_i + \beta_3 \cdot pct\_irrigated_i + \varepsilon_i \tag{2}$$

with forage/pasture as the reference category. Variance inflation factors confirmed the absence of harmful multicollinearity (all VIF < 5). Where OLS residuals were spatially autocorrelated (Moran's I, $p < 0.05$), a spatial error model (SEM) was fitted as the primary inferential model.

The TWFE panel introduced in Section 2.5.2 is estimated over the same 127 sub-watersheds; its non-significant Driscoll-Kraay results (Section 3.5) may appear to undermine the two-stage SEM, but the two approaches ask fundamentally different questions and address distinct statistical quantities. The panel estimates the *pooled mean* $\bar{\beta} = E[\beta_i]$, Driscoll-Kraay SEs make this uncertain because contemporaneous cross-sectional dependence reduces the effective independent information available to pin down the common temporal slope. The SEM, by contrast, uses the *cross-sectional dispersion* of per-sub-watershed slopes β_i, testing whether irrigation-dense sub-watersheds show systematically larger β_i than rainfed sub-watersheds. These are separable quantities, $E[\beta_i]$ can be uncertain while $\mathrm{Var}(\beta_i)$ is real and structured. A concern that per-sub-watershed OLS slopes are "spurious" because they capture a common year-effect conflates these two estimands. When a common drought signal simultaneously depresses SPEI across all sub-watersheds, β_i measures how strongly each sub-watershed's WUE co-moves with that signal, a valid and interpretable measure of local coupling strength. An irrigation-dense sub-watershed with $\beta_i = 0.8$ genuinely shows stronger drought coupling than a rainfed sub-watershed with $\beta_i = 0.1$, regardless of whether the pooled mean is identifiable. Moran's I = 0.514 ($p < 0.001$) on the observed β_i values confirms this cross-sectional variation is spatially organized rather than noise.

A supplementary pre-drought comparison using the 2007 census is reported in Supplementary Table S-9; as detailed in Section 2.4, imputation issues render it uninformative for all three predictors. Robustness was verified through: (i) restriction to within-Csb warm-summer Mediterranean sub-watersheds (n = 67); (ii) a synchronized-time bootstrap (B = 1000) propagating stage-1 estimation uncertainty while preserving cross-sectional spatial covariance (Supplementary Table S-10); (iii) a barren-exclusion dynamic land-cover filter excluding MODIS-confirmed non-vegetated pixels (Supplementary Table S-7); (iv) a parallel SEM using the Standardized Snow Water Equivalent Index (SWEI) from ERA5-Land as the drought predictor (Supplementary Table S-6); and (v) addition of sub-watershed centroid latitude as a direct covariate to test whether the irrigation association persists after explicit control for the latitudinal aridity gradient (Table 1).

2.6. Software

All statistical analyses and spatial processing were conducted in R (v4.5.2; R Core Team (2025)). Raster operations and spatial aggregation used `terra` (v1.8.54; Hijmans (2025)). Vector geometries and spatial joins used `sf` (v1.0.23; Pebesma (2018), Pebesma and Bivand (2023)). Spatiotemporal array operations used `stars` (v0.6.8; Pebesma and Bivand (2023)). Mann-Kendall trend tests and Sen's slope estimation with prewhitening used `modifiedmk` (v1.6; Patakamuri and O'Brien (2021)) and `trend` (v1.1.6; Pohlert (2023)). Spatial autocorrelation (Moran's I, Getis-Ord Gi*) and spatial weight matrices used `spdep` (v1.4.1; Bivand and Wong (2018)). Spatial Error Model was made using `{spatialreg}` (Bivand et al., 2021). Panel regression with fixed effects used `plm` (Croissant and Millo, 2008); Driscoll-Kraay standard errors via `plm::vcovSCC` (Driscoll and Kraay, 1998); HC1 clustered SEs via `plm::vcovHC` with `lmtest::coeftest`. Variance inflation factors used `car` (v3.1.3; Fox and Weisberg (2019)). General-purpose data manipulation and reshaping used `tidyverse` (v2.0.0; Wickham et al. (2019)), including `dplyr`, `tidyr`, `readr`, `stringr`, `purrr`, and `lubridate`. Thematic maps used `tmap` (v4.2; Tennekes (2018)). Statistical graphics used `ggplot2` (v3.5.2; Wickham (2016)). Multi-panel figure layout used `patchwork` (v1.3.1; Pedersen (2025)).

3. Results

3.1. Long-term WUE trends

Trend analysis across 127 Chilean agricultural sub-watersheds revealed predominantly negative WUE trends across the Mediterranean-climate zone (approximately 30°S–35°S), consistent with megadrought onset and intensification (Figure 2).

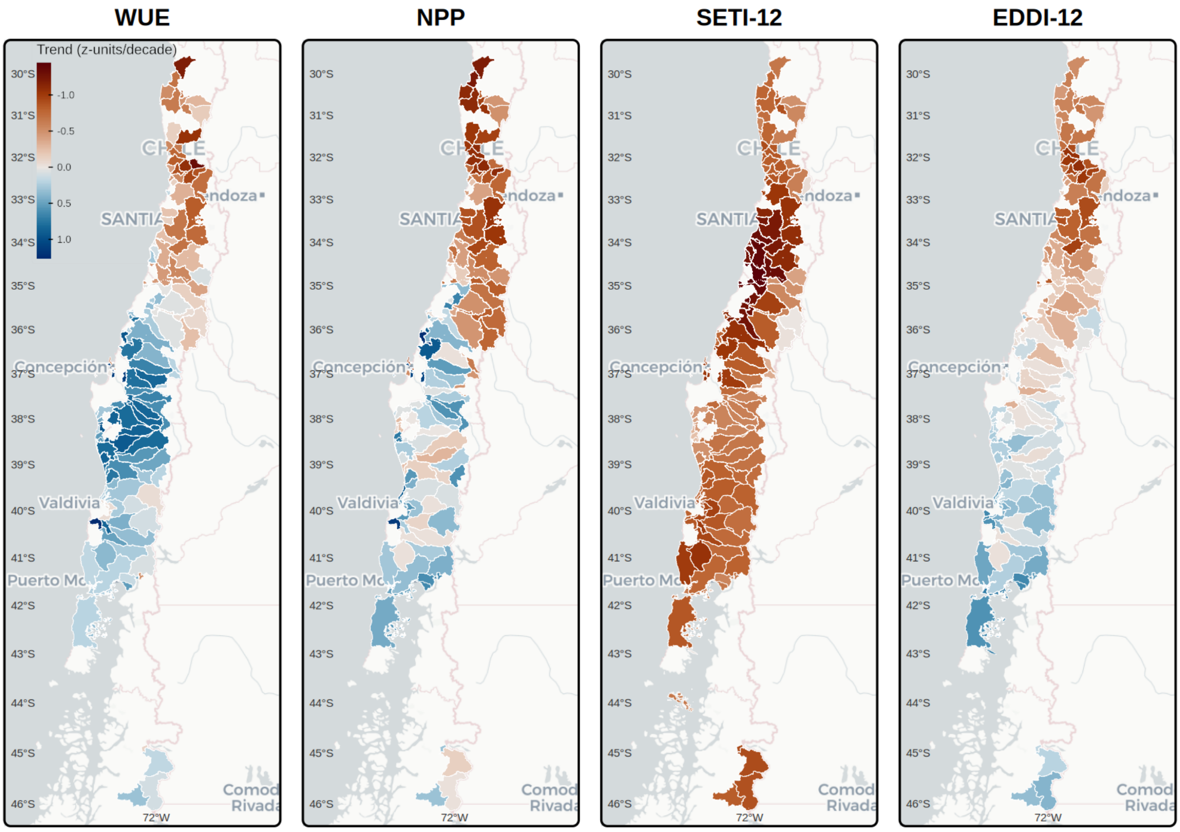

Figure 2: Spatial distribution of long-term trends in zWUE (WUE anomaly), zNPP (NPP anomaly), SETI-12 (12-month ET anomaly), and EDDI-12 (12-month atmospheric evaporative demand) across Chilean sub-watersheds (2001-2020). Trend magnitudes are expressed as z-score standardized Sen's slope estimates.

NPP (MOD17A3HGF) and SETI-12 (MOD16A2GF) are independent proxy products that do not decompose the CASEarth WUE directly; the following patterns are descriptive spatial co-variation, not formal component attribution. NPP trends exhibit strong spatial covariance with WUE, with negative anomalies concentrated in the same central Mediterranean sub-watersheds where WUE declines are most pronounced. SETI-12 trends are more spatially complex: sub-watersheds where ET declined less steeply than NPP tend to show WUE decline, while those where ET reduction exceeded NPP reduction tend toward stable or improving WUE.

Declining WUE is spatially co-located with negative NPP anomalies, while ET responses are heterogeneous and modulated by irrigation access and crop type. Whether NPP suppression is a more proximate correlate of WUE decline than ET cannot be formally established from these proxy data, as the independent products may differ in sensitivity and error structure from the EF-LUE and ETMonitor components underlying the CASEarth WUE (Fifth limitation, Section 4.6).

3.2. WUE change-point analysis

The Pettitt test detected FDR-significant mean-level change points in 22 of 131 sub-watersheds (adjusted p range: 0.019–0.047), all dated 2009–2012. The permutation null model showed that 72.1% of null Pettitt tests also had break years within ±2 years of 2010 (observed: 84.1%); the Kolmogorov-Smirnov test detected no significant difference ($D = 0.153$, $p = 0.255$), a failure to reject the null. The observed break-year concentration near 2010 is therefore not distinguishable from what would be expected under SPEI-step-change tracking alone. Break years were not significantly spatially clustered (Moran's $I = 0.018$, $p = 0.345$), consistent with common large-scale forcing rather than spatial propagation. The geographic distribution of FDR-significant breaks, concentrated in the central Mediterranean zone while the arid north and wet south show no aligned breaks (Boisier et al., 2018; Garreaud et al., 2020), is provided for descriptive reference (Figure 3 a).

3.3. WUE before and after the megadrought

Mapping $\Delta WUE = WUE_{post} - WUE_{pre}$ per sub-watershed revealed pronounced spatial heterogeneity (Figure 3 b). Arid and semi-arid sub-watersheds showed predominantly negative ΔWUE, while irrigated Mediterranean and humid-temperate sub-watersheds showed positive ΔWUE. The aggregate Wilcoxon signed-rank test was positive and significant ($p = 0.007$), but this reflects the numeric dominance of irrigated Mediterranean sub-watersheds, not widespread drought resilience. Köppen-stratified analyses resolve the heterogeneity (Supplementary Table S-2). BW (hot desert; $n = 8$) showed significant declines (Hodges-Lehmann [HL] estimate = -0.535, 95% Confidence Intervals [CI]: -0.862 to -0.335; $p = 0.008$), as did BS (semi-arid steppe; $n = 14$; $HL = -0.643$, $p < 0.001$). Csb (warm-summer Mediterranean; $n = 71$) and Cf (humid subtropical; $n = 26$) exhibited significant WUE increases ($HL = +0.374$, $p < 0.001$ and $HL = +0.367$, $p < 0.001$, respectively). Violin-boxplot distributions stratified by Köppen class (Figure 3 c) confirm this divergence.

3.4. WUE responses to aridification signals

Spearman correlation analysis at the per-family optimal scales (SPEI-12, SPI-12, EDDI-24) revealed positive associations between annual WUE and drought indices across most Chilean sub-watersheds (Figure 4), with

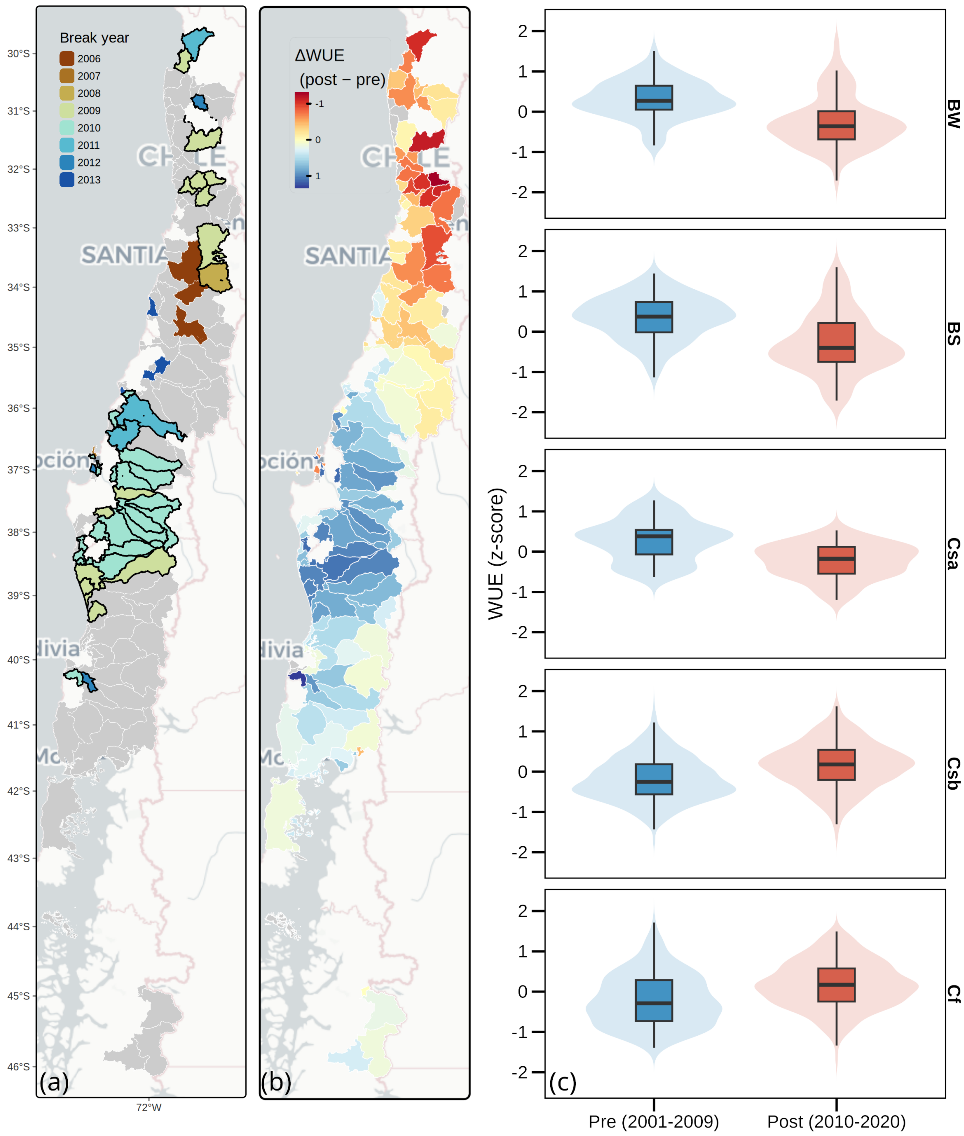

Figure 3: (a) Spatial distribution of Pettitt change-point years in annual WUE per sub-watershed (FDR-significant at adjusted $p < 0.05$). Sub-watersheds with change-point years within ± 2 years of 2010 are highlighted with bold borders. FDR-significant breaks concentrate in the central Mediterranean zone; the permutation null model does not distinguish this concentration from SPEI-step-change tracking (KS $p = 0.255$; Section 3.2). Provided for descriptive geographic reference. Non-significant change points are shown in grey. (b) Spatial map of WUE change between the megadrought period (2010–2020) and the pre-megadrought period (2001–2009) ($\Delta WUE = WUE_{post} - WUE_{pre}$) per sub-watershed. Positive values (blue) indicate net WUE increase; negative values (red) indicate WUE decline. Köppen climate zone boundaries (dashed lines) are overlaid. (c) Violin-boxplot distributions of annual WUE for the pre-megadrought (blue, 2001–2009) and megadrought (red, 2010–2020) periods, stratified by Köppen climate class. Each panel corresponds to one climate class; y-axes are free-scaled.

wetter years generally associated with higher WUE.

At the 36-month scale, SPEI and SPI showed practically equivalent associations with WUE (mean R^2 = 0.240 and 0.229; TOST within ±0.05 margin: $p < 0.001$, 90% CI [−0.004, +0.003]), both significantly outperforming EDDI-36 (mean R^2 = 0.140; $p < 0.001$; Supplementary Figure S-2). The precipitation component dominates the spatial gradient in WUE variability at multi-year accumulation scales.

3.5. Panel regression: temporal WUE-drought relationships

Under Driscoll-Kraay standard errors, no panel coefficient reaches conventional significance at any index or accumulation scale. SPEI-12 ($\beta = -0.112$, DK $p = 0.273$), SPI-12 ($\beta = -0.170$, DK $p = 0.053$), and Mediterranean-restricted SPEI-24 ($\beta = +0.193$, DK $p = 0.458$) and SPI-24 ($\beta = +0.141$, DK $p = 0.579$) are all non-significant (Supplementary Table S-11). The negative signs at the 12-month scale arise from humid-temperate Cf sub-watersheds (n = 26), where rainfed annual systems transiently raise WUE under mild moisture stress (Yu et al., 2020). The substantive interpretation is that WUE-drought co-variation in the temporal panel is largely a spatially common signal. The same calendar years are simultaneously wet or dry across all Mediterranean sub-watersheds, leaving insufficient independent within-unit variation to support inference once cross-sectional dependence is properly accounted for. The drought index's physical role in determining WUE sensitivity is established through the cross-sectional sensitivity slopes (Section 3.6, Section 3.7) and the DGA streamflow validation (Section 4.3), not through the panel temporal analysis. Full HC1 vs. DK comparison is in Supplementary Table S-11. A linear HC1 post-2010 interaction model at SPEI-36 yields a positive intensification term ($\beta = +0.281$, $p = 0.012$; Supplementary Figure S-6), but Supplementary Table S-8 shows this pattern is attributable to the concentration of strongly negative SPEI-36 values after 2010 operating on a concave WUE-SPEI relationship, not a discrete temporal structural break.

3.6. Spatial distribution and clustering of WUE sensitivity

The WUE-SPEI-12 sensitivity map (Figure 5 a) shows the OLS slope per sub-watershed. Sensitivity broadly follows the latitudinal aridity gradient, with central Mediterranean sub-watersheds exhibiting higher values than humid southern sub-watersheds and locally elevated sensitivity in perennial-dominated irrigated zones (Figure 5 b and c).

Moran's I for WUE trend slope was I = 0.683 ($p < 0.001$) and for WUE-SPEI-12 R^2 was I = 0.509 ($p < 0.001$), confirming strong geographic clustering. Getis-Ord Gi* hotspot analysis identified coherent coldspots

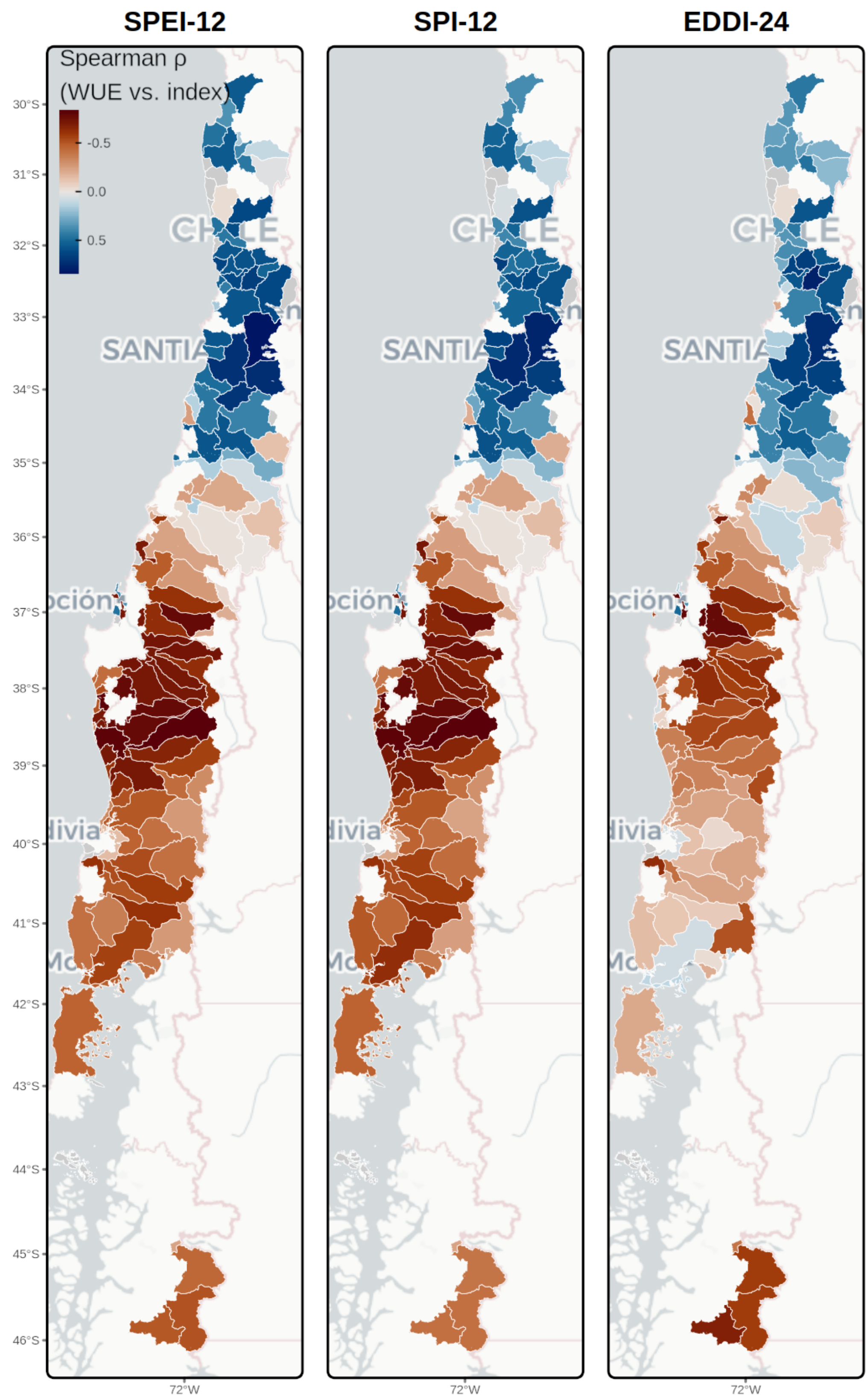

Figure 4: Spatial maps of Spearman (WUE vs. drought index) per sub-watershed, faceted by drought index at the accumulation scales used for the per-sub-watershed spatial analyses (SPEI-12, SPI-12, EDDI-24). Diverging colour scale (blue = positive correlation, red = negative correlation).

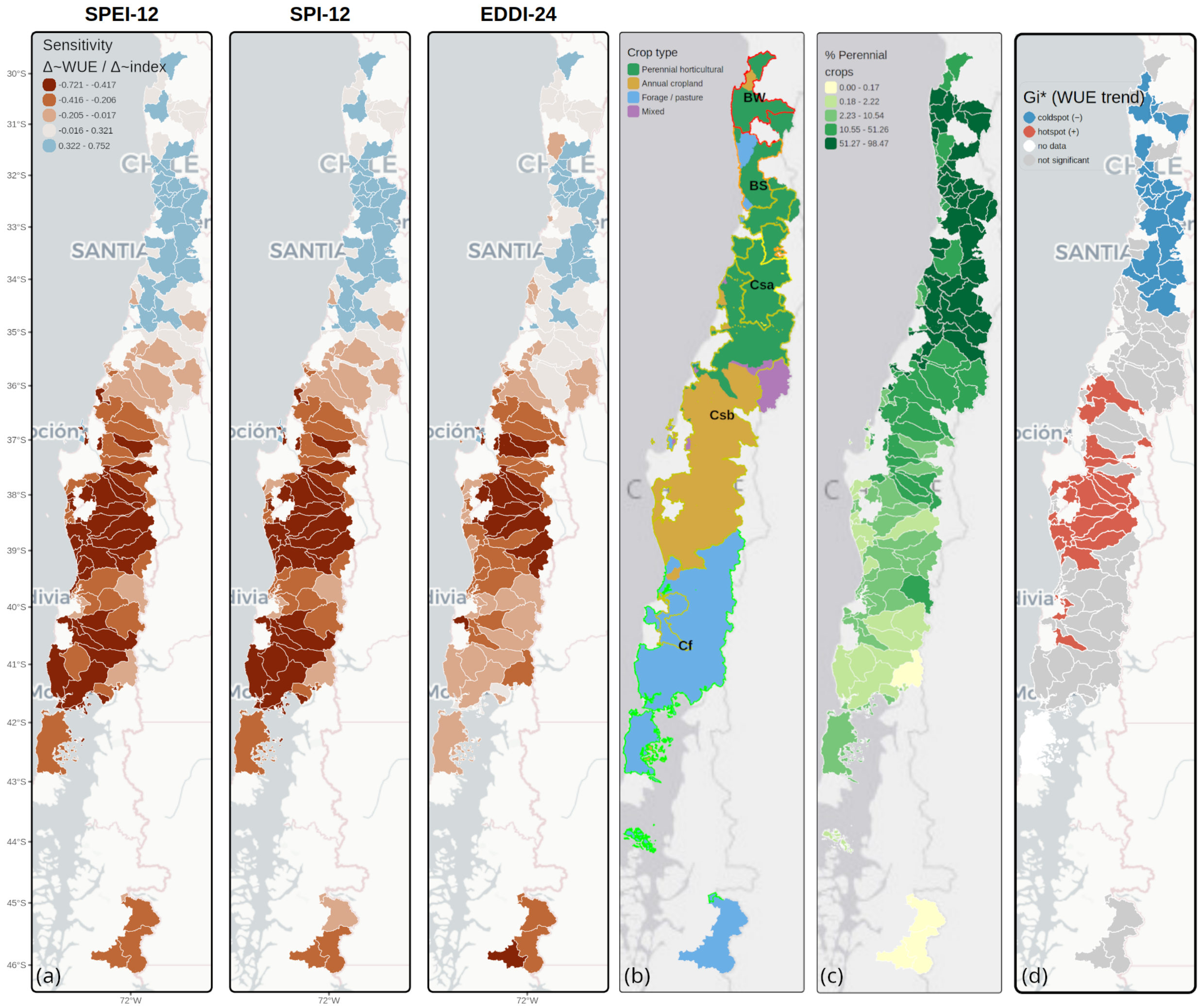

Figure 5: (a) Spatial distribution of WUE-drought sensitivity ($\Delta WUE/\Delta Index$, the OLS slope of the annual WUE ~ index regression per sub-watershed, 2001-2020) for SPEI-12, SPI-12, and EDDI-24. High positive values indicate strong positive WUE response; near-zero or negative values indicate weak or inverted coupling. (b) Choropleth map of dominant crop type per sub-watershed, classified by the agricultural functional group exceeding 40% of total agricultural area (Perennial horticultural, Annual cropland, Forage/pasture, Mixed). (c) Choropleth map of perennial crop share (% of total agricultural area under fruit trees and vineyards) per sub-watershed. (d) Getis-Ord Gi* hotspot analysis of WUE trend slope across Chilean sub-watersheds. Red sub-watersheds are statistically significant hotspots (positive WUE trend clusters; Gi* > 1.96); blue are coldspots (negative WUE trend clusters; Gi* < -1.96); grey are not significant at the 95% level.

in the central Mediterranean zone and localized hotspots in transitional zones (Figure 5 d). Pettitt change-point years were not significantly spatially clustered (I = 0.018, p = 0.345), indicating that the temporal concentration near 2010 reflects common large-scale forcing rather than spatial propagation. Hydroclimate governs when and how strongly WUE shifts over time; crop composition modulates the spatial magnitude of each sub-watershed's drought sensitivity. These two axes are complementary rather than competing.

3.7. Agricultural crop composition and WUE sensitivity

Integration of census-derived crop composition with WUE-SPEI-12 sensitivity estimates (n = 127 sub-watersheds) revealed contrasting patterns by crop system. Annual cropland sub-watersheds showed lower sensitivity than forage/pasture watersheds, while perennial horticultural sub-watersheds showed the highest median sensitivity (Figure 6 a); because perennial crop distribution, aridity, and WUE sensitivity all co-vary with latitude (Figure 7 c), the perennial pattern likely reflects the underlying climate gradient rather than an isolated crop-system effect (Section 4.6). Irrigated area share was positively associated with sensitivity in the full-sample pooled analysis (Figure 7 a).

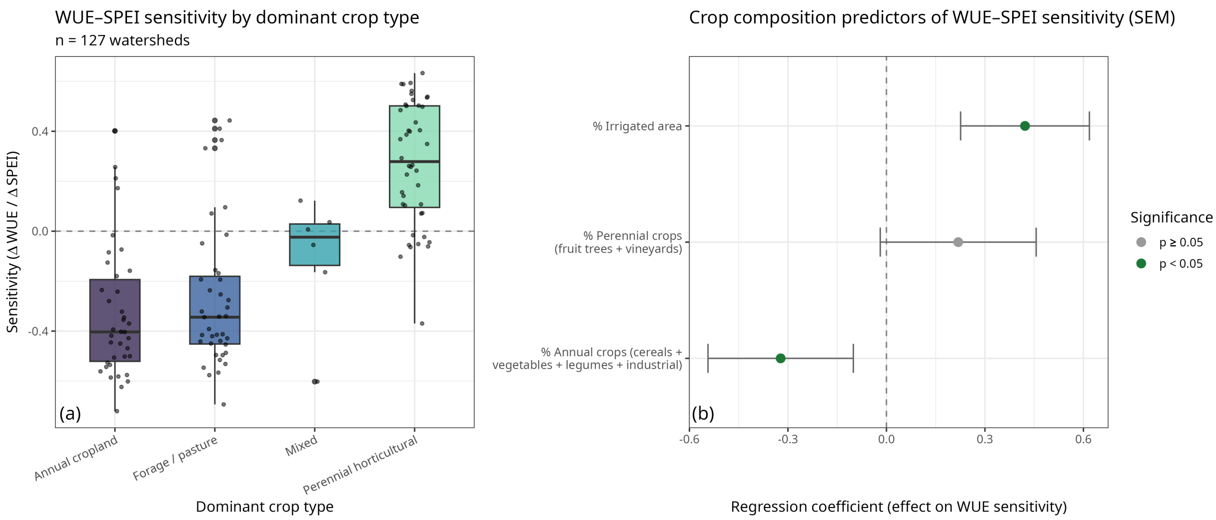

Figure 6: WUE-SPEI-12 sensitivity by dominant crop type (n = 127 sub-watersheds). (a) Boxplot distributions of per-sub-watershed OLS sensitivity slopes stratified by dominant agricultural system: perennial horticultural (fruit trees + vineyards), annual cropland (cereals + vegetables + legumes + industrial crops), mixed systems (no single group exceeds 40% of agricultural area), and forage/pasture. Perennial-dominated sub-watersheds show the highest median sensitivity; forage/pasture sub-watersheds show the lowest. (b) Full-sample SEM coefficient plot for the three functional-aggregate predictors (perennial crops, annual crops, irrigated area; reference: forage/pasture) with 95% confidence intervals; filled symbols indicate p < 0.05. Numeric values and within-Csb comparisons are in Table 1.

The multivariate OLS regression (n = 127 sub-watersheds) returned annual crop share as a significant negative predictor ($\beta = -0.304$, $p < 0.001$), indicating buffering relative to the forage/pasture reference; perennial crop share as a positive but subsequently attenuated predictor ($\beta = 0.359$, $p = 0.003$); and irrigated area share as the strongest positive predictor ($\beta = 0.499$, $p < 0.001$), reflecting the association between irrigation infrastructure prevalence and drought coupling rather than actual water volumes delivered in drought years.

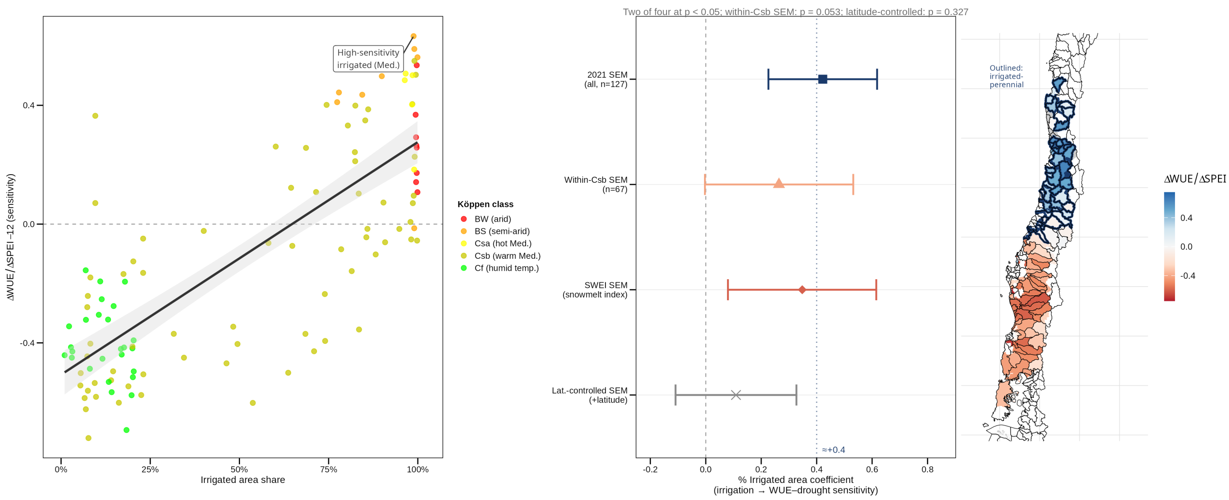

Figure 7: (a) Scatter plot of WUE-SPEI-12 sensitivity versus irrigated area share per sub-watershed (n = 127), coloured by Köppen climate class, with a pooled OLS regression line (±95% CI). Points in the upper-right cluster (high irrigation, high sensitivity) correspond to Mediterranean irrigated-perennial systems; points in the lower-left correspond to rainfed or annual-crop dominated systems. (b) Forest plot of the irrigated area share regression coefficient (±95% CI) across four model specifications: 2021 full-sample SEM, within-Csb warm-summer Mediterranean SEM, SWEI-based SEM using snowmelt index as the drought predictor, and a latitude-controlled SEM with sub-watershed centroid latitude added as a covariate. The 2007 pre-drought SEM is omitted from this figure because imputation issues render it uninformative (Supplementary Table S-9). Two specifications are significant at $p < 0.05$ (full-sample SEM and SWEI SEM); the within-Csb SEM is marginal (= +0.264, p = 0.053); the latitude-controlled SEM attenuates to = +0.109 (p = 0.327), consistent with partial confounding by the latitudinal aridity gradient. The vertical dotted line marks +0.4 for reference. (c) Choropleth of WUE-SPEI-12 sensitivity (OLS slope per sub-watershed, 2001–2020); solid blue borders outline perennial-horticultural-dominant sub-watersheds, which concentrate in the central Mediterranean zone and correspond to the high-sensitivity cluster in panel (a).

Moran's I on OLS residuals was I = 0.197 ($p = 0.001$), so a spatial error model (SEM; queen-contiguity weights) was fitted as the primary inferential model ($\lambda = 0.468$, $p < 0.001$). The SEM attenuated but largely preserved the OLS conclusions: annual crop share ($\beta = -0.322$, $p = 0.004$), perennial crop share ($\beta = 0.219$, nominal $p = 0.071$; Figure 6 b), and irrigated area share ($\beta = 0.422$, $p < 0.001$). A synchronized-time bootstrap (Supplementary Table S-10) confirmed significance for all three predictors ($p = 0.002$-0.032) with bootstrap SEs 0.74-0.91× nominal; WLS estimates (Supplementary Table S-5) confirm no sign changes under stage-1 uncertainty weighting.

To test whether associations are crop-system properties robust to the latitudinal aridity gradient, the model was restricted to Csb warm-summer Mediterranean sub-watersheds (n = 67). Results differ strikingly by predictor (Table 1):

Table 1. Comparison of WUE-SPEI-12 sensitivity regressions across model specifications. Full-sample SEM: n = 127 (all climate classes); within-Csb OLS and SEM: n = 67 (warm-summer Mediterranean, $\lambda = 0.255$, $p = 0.057$); latitude-controlled SEM: n = 127 with sub-watershed centroid latitude added as a covariate. Reference category: forage/pasture. *** $p < 0.001$; ** $p < 0.01$; * $p < 0.05$; † $p < 0.10$. Full model outputs in Supplementary Tables S-4 (within-Csb) and S-14 (latitude-controlled).

Predictor	Full-sample SEM	Full-sample SEM p	Within-Csb OLS β	Within-Csb OLS p	Within-Csb SEM β	Within-Csb SEM p	Lat.-controlled SEM β	Lat.-controlled SEM p
% Irrigated area	+0.422	< 0.001 ***	+0.317	0.016 *	+0.264	0.053 †	+0.109	0.327
% Annual crops	−0.322	0.004 **	−0.463	0.004 **	−0.565	0.001 **	−0.485	< 0.001 ***
% Perennial crops	+0.219	0.071 †	+0.297	0.102	+0.184	0.320	+0.025	0.833

The annual-crops association strengthens within Csb (SEM $\beta = -0.565$, $p = 0.001$), confirming it as a genuine crop-system property independent of the latitudinal gradient. Perennial crop share is non-significant in all specifications (full-sample SEM $p = 0.071$; within-Csb SEM $p = 0.320$), consistent with its inseparability from the latitudinal aridity gradient. The irrigated area association survives the Csb restriction in OLS ($\beta = +0.317$, $p = 0.016$), attenuating to marginal significance under SEM within Csb ($\beta = +0.264$, $p = 0.053$; Figure 7 b).

A direct latitude-control test, adding sub-watershed centroid latitude as a covariate to the full-sample SEM, is presented in Table 1 (rightmost columns). The irrigation coefficient attenuates from $\beta = +0.422$ to $\beta = +0.109$ ($p = 0.327$; ΔAIC = 20.4), confirming partial confounding with the latitudinal aridity gradient. The annual-crops coefficient strengthens ($\beta = -0.485$, $p < 0.001$), establishing annual-crop buffering as the more latitude-robust result. The perennial coefficient collapses to near zero ($\beta = +0.025$, $p = 0.833$).

The pre-drought census comparison is reported in Supplementary Table S-9; imputation issues render it uninformative for distinguishing structural from adaptive effects (Section 2.4). The causal direction of the 2021 negative association is discussed in Section 4.3.

Natural vegetation contamination within the agricultural mask was non-significant as a control covariate ($\beta = 0.098$, $p = 0.509$; Supplementary Figure S-3).

4. Discussion

4.1. The megadrought as a driver of persistent WUE change

WUE undergoes a mean-level shift concurrent with the megadrought onset is a physically expected consequence of WUE being hydroclimate-driven, not a novel finding. The permutation null model provides no evidence to distinguish the observed break-year concentration from simple SPEI step-change tracking (KS p = 0.255), confirming this expectation. The geographic distribution of FDR-significant breaks, concentrated in the central Mediterranean zone, is descriptively consistent with megadrought forcing but does not establish coupling beyond what SPEI-step-change tracking alone would produce. The aggregate WUE increase (Wilcoxon p = 0.007) masks pronounced spatial heterogeneity. Arid northern sub-watersheds declined while the irrigated Mediterranean zone rose, coinciding with the elevated drought coupling documented in Section 4.3.

4.2. Multidimensional aridification: why index choice matters

The practically equivalent performance of SPEI-36 and SPI-36 in cross-sectional analyses (TOST: $p < 0.001$) indicates that the precipitation component dominates the spatial gradient in WUE sensitivity under megadrought conditions. The TWFE panel provides no statistically significant evidence for within-unit temporal WUE-drought coupling at any index or scale once cross-sectional dependence is accounted for through Driscoll-Kraay SEs (Supplementary Table S-11). The substantive interpretation is that WUE-drought co-variation in the temporal panel is largely a spatially common phenomenon. The same calendar years are wet or dry across all Mediterranean sub-watersheds simultaneously, leaving insufficient independent within-unit variation to support inference. Drought's physical role in determining WUE sensitivity is established through the cross-sectional sensitivity slopes and the DGA streamflow validation, not through the panel temporal analysis.

4.3. Irrigation infrastructure and WUE drought sensitivity

In the full-sample SEM, irrigated area share is positively associated with WUE-drought sensitivity ($\beta = +0.422$, $p < 0.001$), with snowmelt co-variation supported by ρ(SPEI-12, DGA streamflow) = 0.72-0.83 and

ρ(streamflow, WUE) = 0.38-0.68 in the three northern basins (Supplementary Table S-13). Adding centroid latitude attenuates this to non-significance ($\beta = +0.109$, $p = 0.327$; Table 1), while the within-Csb restriction retains a marginal association ($\beta = +0.264$, $p = 0.053$). The evidence does not contradict demand-hardening dynamics (Grafton et al., 2018; Ward and Pulido-Velázquez, 2008) but cannot establish the irrigation association as latitude-independent.

The annual-crops association is robust to latitude control, strengthening from $\beta = -0.322$ to $\beta = -0.485$ when latitude is added (Table 1); the causal direction is ambiguous and is addressed in limitation (vii, Section 4.6).

The perennial crop coefficient is non-significant in all specifications (full-sample p = 0.071; within-Csb SEM p = 0.320; latitude-controlled p = 0.833; Table 1), most plausibly reflecting statistical inseparability from the irrigation coefficient in Chile's Mediterranean zone, where irrigation enables perennial cultivation that creates inelastic water demand (Grafton et al., 2018). Both associations are hypotheses consistent with the data, each constrained by a distinct confound, and should not be interpreted as established causal mechanisms (Boser et al., 2024; FAO y ONU Agua, 2025; Hellegers and Van Halsema, 2021; Wang et al., 2024).

4.4. Spatial structure, global implications, and limits of adaptation

WUE coldspots are concentrated in the Aconcagua, Maipo, Rapel, Mataquito, and Maule basins (32-36°S), precisely the zone concentrating Chile's export fruit and wine production. Because the central agricultural corridor stresses simultaneously, water-market transfers under Chile's privatized Water Code have limited scope to buffer basin-scale shortfalls (Budds, 2020; Malagueño and D'Odorico, 2024; Rivera et al., 2016). Drought-driven WUE decline means more water is consumed per unit of biomass produced; sustaining production in high-sensitivity basins requires proportionally greater withdrawals precisely when supply is lowest.

The supply-failure mechanism applies conceptually to snowmelt-dependent irrigated agriculture globally (Barnett et al., 2008; Immerzeel et al., 2020; Lutz et al., 2014), but the quantitative crop composition model is a within-Chile spatial descriptor and does not transfer geographically (Figure 8); the mechanism is portable, the coefficients are not. Institutional buffering capacity also differs substantially. Chile's privatized water market, where simultaneous basin-scale droughts exhaust reallocation capacity, represents one end of a governance spectrum, while state-managed systems with groundwater banking may partially decouple farm-gate delivery from meteorological signals.

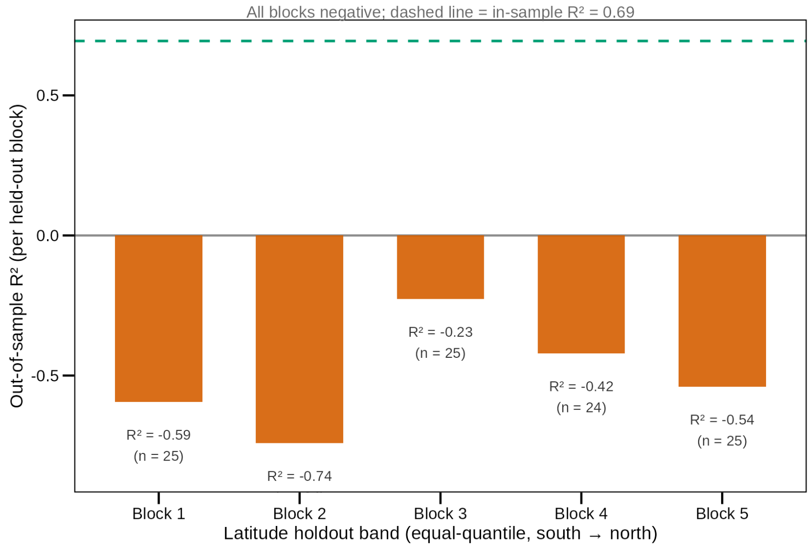

Figure 8: Geographic cross-validation of the crop composition-WUE-SPEI-12 sensitivity model. Continental Chile was partitioned into five equal-latitude-quantile holdout bands (ordered south to north); each band was predicted from a model trained on the remaining four. All five per-block out-of-sample R^2 values are negative (range -1.56 to -0.30), well below the in-sample R^2 of 0.69 (dashed line), meaning the model predicts a held-out latitude band worse than that band's own mean. The quantitative coefficients are not geographically portable; only the supply-failure mechanism transfers conceptually to other snowmelt-dependent irrigation systems.

Where irrigation supply is hydrologically coupled to the same climate signals that drive drought, expanding irrigation infrastructure without securing supply independence may increase aggregate drought exposure. This does not argue against irrigation per se, but distinguishes between systems with independent supply and those coupled to snowmelt and precipitation, a distinction with direct relevance for investment prioritization and drought-contingency planning (FAO y ONU Agua, 2025).

The coldspot concentration in the five key basins is quantifiable in terms directly relevant to water allocation and planting decisions. Sub-watersheds in the Aconcagua and Maipo basins show the highest mean WUE-SPEI-12 sensitivities in the dataset (mean $\beta = 0.45$ and 0.54 respectively; individual sub-watershed peaks of 0.50 and 0.63), combined with near-complete irrigation infrastructure prevalence (mean pct_irrigated > 0.97) and confirmed hydrological coupling (ρ(SPEI-12, streamflow) $= 0.75$ and 0.82; ρ(streamflow, WUE) $= 0.61$ and 0.68). These basins concentrate Chile's export fruit and wine production under a regime where rights granted by the 1981 Water Code are permanent and freely tradeable, but where basin-scale reallocation cannot buffer a deficit that reduces supply for all rights holders simultaneously (Budds, 2020; Rivera et al., 2016). By contrast, Mataquito and Maule sub-watersheds show markedly lower mean sensitivities (0.12 and -0.03) despite similarly high irrigation prevalence (mean pct_irrigated 0.96 and 0.92), consistent with greater rainfall supplementation of snowmelt at higher latitudes. This north-to-south gradient implies that the lock-in risk of new perennial investment is not uniform across the Mediterranean zone. The same commitment to perennial horticulture or viticulture that carries moderate coupling risk in Maule carries substantially higher coupling risk in Aconcagua and Maipo, where meteorological drought and surface-water supply failure are most tightly linked. Under a sustained aridification trend, water-rights allocation frameworks that do not account for basin-level hydrological coupling may systematically underestimate the structural demand gap that long-horizon perennial commitments create.

These findings carry different implications depending on whether the management horizon is framed around transient drought or prolonged aridification. Contingency responses (groundwater banking, interbasin reallocation, reservoir buffering) cannot resolve structural exposure under directional aridification, because supplementary reserves are progressively depleted when below-normal conditions become the persistent baseline. Expanding snowmelt-dependent irrigation infrastructure or establishing new perennial orchards and vineyards during an ongoing aridification trend deepens crop-system lock-in, committing a watershed to inflexible water demand at precisely the timescale at which aridification operates. Conversely, annual-crop portfolio flexibility is associated with lower sensitivity and preserves capacity to adjust planted area during sustained supply deficits. WUE-based efficiency metrics are insufficient indicators of resilience under aridification. Efficiency gains do not reduce supply coupling, and supply independence and crop-portfolio flexibility are the structural properties that differentiate lower-sensitivity from higher-sensitivity systems.

4.5. Ecosystem WUE and agronomic WUE: interpreting biophysical signals in an agricultural context

The metric analyzed throughout this study, $WUE_{eco} = NPP/ET$ (g C kg^{-1} H_2O yr^{-1}), quantifies ecosystem-scale carbon assimilation efficiency per unit of total water loss, integrating soil evaporation, canopy transpiration, and the full phenological cycle across the sub-watershed footprint (Beer et al., 2010; Ito and Inatomi, 2012). This is conceptually distinct from agronomic WUE (WUE_{agro}), defined as harvestable yield per unit of water supplied or consumed (Stanhill, 1986; Zwart and Bastiaanssen, 2004). WUE_{eco} is a biophysical ecosystem property appropriate for regional remote sensing monitoring and cross-site structural comparison; WUE_{agro} is a production ratio conditioned on crop-specific biomass partitioning, harvest timing, and management decisions operating below the spatial resolution at which WUE_{eco} is observed. The two metrics should not be treated as interchangeable, and changes in one do not imply proportional changes in the other.

The theoretical linkage between WUE_{eco} and WUE_{agro} runs through the harvest index (HI, the fraction of above-ground NPP allocated to harvestable organs) and the transpiration fraction of total ET: $WUE_{agro} \approx$

$WUE_{eco} \times (HI/f_{T/ET})$. Under water stress, both parameters are unstable in crop-type-specific ways. In annual cereals and legumes, mild deficit can increase HI by accelerating reproductive development, partially decoupling WUE_{agro} from WUE_{eco} trajectories, whereas severe drought suppresses HI through grain abortion while soil evaporation sustains ET above levels proportional to biomass production (Fereres and Soriano, 2006; Sinclair, 1998). In perennial tree crops and vineyards, multi-year carbon allocation to structural woody biomass means annual NPP does not map onto harvestable productivity within the same growing season. This may partly explain the non-significant perennial coefficient across all model specifications (full-sample SEM p = 0.071; within-Csb p = 0.320; Table 1), reflecting the indirect and temporally lagged linkage between perennial-system WUE_{eco} and single-year harvestable output, compounded by collinearity with the irrigation variable.

The positive aggregate ΔWUE in irrigated Mediterranean sub-watersheds (Wilcoxon p = 0.007) is consistent with three non-exclusive mechanisms: maintained irrigation supply sustaining NPP while rainfed vegetation declines; drought-induced stomatal up-regulation increasing intrinsic WUE under rising vapor pressure deficit (Keenan et al., 2013; Medlyn et al., 2011); and rising atmospheric CO_2 over the study window independently increasing intrinsic WUE through partial stomatal closure (Keenan et al., 2013). Because the CASEarth dataset does not distribute internal component layers (limitation v, Section 4.6), formal attribution among these contributions is not feasible. The critical implication is that positive WUE_{eco} does not indicate agronomic resilience: a system maintaining high NPP/ET under increasing irrigation inputs may simultaneously reduce WUE_{agro} if water application rises faster than yield, reproducing the efficiency paradox at the landscape scale (Grafton et al., 2018). The buffered WUE sensitivity of annual-dominated sub-watersheds (SEM $\beta = -0.322$, p = 0.004) carries a parallel ambiguity: annual systems can contract planted area proportionally under supply deficit, stabilizing NPP/ET even as production volume declines. Whether this reflects structural portfolio flexibility or drought-driven abandonment cannot be established from the cross-sectional design alone (limitation vii), and the two interpretations carry opposite agronomic implications.

WUE_{eco} is a robust and spatially scalable indicator for detecting shifts in ecosystem carbon-water coupling that would be undetectable from yield statistics alone, and is the appropriate metric for the structural comparisons undertaken here. It should not, however, be deployed as a proxy for WUE_{agro} in policy discourse without explicit crop-type stratification, harvest index estimation, and calibration against yield census data. The Chilean patterns expose where ecosystem functioning has been most strongly disrupted by prolonged aridification and which land-use structural properties modulate that disruption. Whether these trajectories translate into proportional agronomic losses requires integration of interannual yield census data at the sub-watershed scale, representing the necessary next step for translating WUE_{eco} signals into actionable inference for water allocation and agricultural planning.

4.6. Methodological limitations and future directions

All findings are associative, derived from cross-sectional observational data. The paired-census quasi-experimental design provides evidence against drought-driven adaptive confounding but cannot establish that irrigation infrastructure is associated with heightened WUE sensitivity through a causal pathway. Findings should be interpreted as structurally stable associations consistent with the proposed mechanisms.

Key limitations are: (i) the static agricultural mask may integrate natural vegetation patches, though matorral contamination was non-significant as a covariate and a barren-exclusion filter confirmed results (Supplementary Table S-7); (ii) the latitudinal gradient is the primary limitation for the irrigation result: adding centroid latitude attenuates the irrigation coefficient to non-significance (Table 1; Figure 8), while the annual-crops association strengthens, establishing it as the more latitude-robust result; (iii) *pct_irrigated* does not distinguish surface from groundwater irrigation, though DGA streamflow validation and aquifer co-decline evidence (Donoso, 2018) make groundwater confounding unlikely; (iv) spatial collinearity between irrigation and perennial crop share prevents isolation of a perennial-specific effect; non-significance of *pct_perennials* likely reflects collinearity rather than an absent pathway; (v) the CASEarth WUE dataset does not distribute component layers, so no formal NPP/ET attribution is presented; (vi) the 2007 census comparison is limited by imputation quality and is reported in Supplementary Table S-9 only; (vii) the cross-sectional design cannot establish the causal direction of the annual-crops association. The negative sign in 2021 (drought-sensitive sub-watersheds have fewer annuals) is consistent with both structural buffering and drought-driven abandonment of annual cultivation; longitudinal data would allow discrimination between these mechanisms (Chakraborti et al., 2023; Xie et al., 2023).

5. Conclusions

Across 127 Chilean agricultural sub-watersheds (2001-2020), four principal conclusions emerge:

1. WUE decline is spatially concentrated in the central Mediterranean zone, co-located with NPP suppression (descriptive co-variation only). Negative trends and structural breaks both concentrate in the 30°S-35°S band.

2. SPEI and SPI carry practically equivalent cross-sectional information about WUE drought sensitivity (TOST equivalence $p<0.001$). Precipitation dominates the spatial gradient in WUE sensitivity at multi-year scales.
3. Annual crop share is robustly negatively associated with drought sensitivity across all latitude specifications (SEM $\beta = -0.322$ to -0.565, $p<0.01$). The negative sign is consistent with both structural buffering and drought-driven abandonment; causal direction cannot be established.
4. Irrigation infrastructure prevalence is positively associated with WUE-drought sensitivity in the full sample ($\beta=+0.422$, $p<0.001$), but this association attenuates substantially when latitude is controlled ($\beta=+0.109$, $p=0.327$) and cannot be statistically isolated from the latitudinal aridity gradient. The evidence is consistent with demand-hardening theory but does not establish it.

Both crop-composition patterns are hypotheses warranting longitudinal validation. Neither can be treated as an established causal mechanism; effective governance under aridification requires explicit accounting for whether irrigation supply is genuinely decoupled from the same hydroclimatic signals that suppress crop productivity.

6. Funding

The National Research and Development Agency of Chile (ANID) funded this study through the drought emergency project FSEQ210022, Fondecyt Iniciación N°11190360, and Fondecyt Iniciación N°11230334. We declare that the authors have no competing interests, or other interests that might be perceived to influence the results and/or discussion reported in this paper.

7. Acknowledgements

The authors acknowledge the use of the CASEarth global cropland WUE dataset (Jiang et al., 2025), MODIS Terra products (MOD17A3HGF, MOD16A2GF) distributed by NASA Earthdata, CHIRPS v2.0 precipitation data and CHIRTS-daily temperature data provided by the Climate Hazards Center (University of California, Santa Barbara), and ERA5-Land reanalysis data provided by the European Centre for Medium-Range Weather Forecasts (ECMWF) via the Copernicus Climate Change Service (used for SWEI derivation). Agricultural census microdata were obtained from the Chilean Instituto Nacional de Estadísticas (INE). The authors declare no conflicts of interest.

8. Code and Data Availability

All analysis code is publicly available at https://github.com/frzambra/WUE_article (R scripts for all preprocessing, statistical analysis, and figure generation steps, with package versions managed via `renv` for reproducibility), enabling immediate reviewer access during manuscript evaluation. A permanent citable archive with a DOI will be deposited at Zenodo upon acceptance.

Annual cropland WUE rasters (NPP/ET, 1 km, 2001-2020) were obtained from Jiang et al. (2025), available at the CASEarth Data Platform (https://data.casearth.cn/dataset/640f0132819aec3f2b52a4bb). NPP data (zNPP) were obtained from MOD17A3HGF (MODIS Terra, 500 m, Collection 6.1) for descriptive trend comparison only. ET anomaly data (SETI-12 December) were derived from MOD16A2GF (MODIS Terra, 500 m 8-day, Collection 6.1) for descriptive trend analysis only; no formal component attribution is presented as independent MODIS proxies do not algebraically reproduce the CASEarth WUE. For cross-product validation purposes, annual ET (zET) was additionally obtained from MOD16A3GF (MODIS Terra, 500 m annual, Collection 6.1; Supplementary Figure S-7). All MODIS products are available from NASA Earthdata (https://earthdata.nasa.gov). Drought index raster time series (SPEI, SPI, EDDI) were computed from CHIRPS v2.0 monthly precipitation (Funk et al., 2015) and CHIRTS-daily temperature (Funk et al., 2019), with SPEI and EDDI using FAO-56 Penman-Monteith reference evapotranspiration derived from CHIRTS. Snow Water Equivalent Index (SWEI) was derived from ERA5-Land monthly snow water equivalent reanalysis data. Agricultural census microdata for the 2007 and 2020-2021 censuses are publicly available from the Chilean Instituto Nacional de Estadísticas (INE; https://www.ine.gob.cl). Full software version details are listed in Section 2.6.

Declaration of generative AI and AI-assisted technologies in the manuscript preparation process

During the preparation of this work, the authors used Claude (Anthropic) to assist with the statistical analysis and to improve the English grammar. After using this tool, the authors reviewed and edited the content as needed and took full responsibility for the published article.

References

AghaKouchak, A., Farahmand, A., Melton, F.S., Teixeira, J., Anderson, M.C., Wardlow, B.D., Hain, C.R., 2015. Remote sensing of drought: Progress, challenges and opportunities. Reviews of Geophysics 53, 452–480. doi:10.1002/2014RG000456.

Barnett, T.P., Pierce, D.W., Hidalgo, H.G., Bonfils, C., Santer, B.D., Das, T., Bala, G., Wood, A.W., Nozawa, T., Mirin, A.A., et al., 2008. Human-induced changes in the hydrology of the western United States. Science 319, 1080–1083. doi:10.1126/science.1152538.

Beer, C., Reichstein, M., Tomelleri, E., Ciais, P., Jung, M., Carvalhais, N., Rödenbeck, C., Arain, M.A., Baldocchi, D., Bonan, G.B., Bondeau, A., Cescatti, A., Lasslop, G., Lindroth, A., Lomas, M., Luyssaert, S., Margolis, H., Oleson, K.W., Roupsard, O., Veenendaal, E., Viovy, N., Williams, C., Woodward, F.I., Papale, D., 2010. Terrestrial Gross Carbon Dioxide Uptake: Global Distribution and Covariation with Climate. Science 329, 834–838. URL: https://www.science.org/doi/10.1126/science.1184984, doi:10.1126/science.1184984.

Bivand, R., Millo, G., Piras, G., 2021. A Review of Software for Spatial Econometrics in R. Mathematics 9, 1276. URL: https://www.mdpi.com/2227-7390/9/11/1276, doi:10.3390/math9111276.

Bivand, R., Wong, D.W.S., 2018. Comparing implementations of global and local indicators of spatial association. TEST 27, 716–748. doi:10.1007/s11749-018-0599-x.

Boisier, J., Alvarez-Garreton, C., Cordero, R., Damiani, A., Gallardo, L., Garreaud, R., Lambert, F., Ramallo, C., Rojas, M., Rondanelli, R., 2018. Anthropogenic drying in central-southern chile evidenced by long-term observations and climate model simulations. Elementa 6, 74. doi:10.1525/elementa.328.

Boser, A., Caylor, K., Larsen, A., Pascolini-Campbell, M., Reager, J., Carleton, T., 2024. Field-scale crop water consumption estimates reveal potential water savings in california agriculture. Nature Communications 15, 2366. doi:10.1038/s41467-024-46031-2.

Budds, J., 2020. Securing the market: Water security and the internal contradictions of chile's water code. Geoforum 113, 165–175. doi:10.1016/j.geoforum.2018.09.027.

Chakraborti, R., Davis, K.F., DeFries, R., Rao, N.D., Joseph, J., Ghosh, S., 2023. Crop switching for water sustainability in india's food bowl yields co-benefits for food security and farmers' profits. Nature Water 1, 864–878. doi:10.1038/s44221-023-00135-z.

Croissant, Y., Millo, G., 2008. Panel data econometrics in R: The plm package. Journal of Statistical Software 27, 1–43. doi:10.18637/jss.v027.i02.

Davis, K., Rulli, M., Seveso, A., D'Odorico, P., 2017. Increased food production and reduced water use through optimized crop distribution. Nature Geoscience 10, 919–924. doi:10.1038/s41561-017-0004-5.

Donoso, G. (Ed.), 2018. Water Policy in Chile. Springer International Publishing, Cham. doi:10.1007/978-3-319-76702-4. global Issues in Water Policy, Vol. 21.

Driscoll, J.C., Kraay, A.C., 1998. Consistent covariance matrix estimation with spatially dependent panel data. Review of Economics and Statistics 80, 549–560. doi:10.1162/003465398557825.

FAO y ONU Agua, 2025. Progreso del cambio en la eficiencia del uso del agua. doi:10.4060/cd2023es.

Fereres, E., Soriano, M.A., 2006. Deficit irrigation for reducing agricultural water use. Journal of Experimental Botany 58, 147–159. URL: https://academic.oup.com/jxb/article-lookup/doi/10.1093/jxb/erl165, doi:10.1093/jxb/erl165.

Fox, J., Weisberg, S., 2019. An R Companion to Applied Regression. 3 ed., Sage, Thousand Oaks, CA.

Funk, C., Peterson, P., Landsfeld, M., Pedreros, D., Verdin, J., Shukla, S., Husak, G., Rowland, J., Harrison, L., Hoell, A., et al., 2015. The climate hazards infrared precipitation with stations—a new environmental record for monitoring extremes. Scientific Data 2, 1–21. doi:10.1038/sdata.2015.66.

Funk, C., Peterson, P., Peterson, S., Shukla, S., Davenport, F., Michaelsen, J., Knapp, K.R., Landsfeld, M., Husak, G., Harrison, L., et al., 2019. A high-resolution 1983–2016 t_{max} climate data record based on infrared temperatures and stations by the climate hazard center. Journal of Climate 32, 5639–5658. doi:10.1175/JCLI-D-18-0698.1.

Garreaud, R., Boisier, J., Rondanelli, R., Montecinos, A., Sepúlveda, H., Veloso-Aguila, D., 2020. The central chile mega drought (2010–2018): A climate dynamics perspective. International Journal of Climatology 40, 421–439. doi:10.1002/joc.6219.

Gebrechorkos, S.H., Sheffield, J., Vicente-Serrano, S.M., Funk, C., Miralles, D.G., Peng, J., Dyer, E., Talib, J., Beck, H.E., Singer, M.B., Dadson, S.J., 2025. Warming accelerates global drought severity. Nature doi:10.1038/s41586-025-09047-2.

Grafton, R.Q., Williams, J., Perry, C.J., Molle, F., Ringler, C., Steduto, P., Udall, B., Wheeler, S.A., Wang, Y., Garrick, D., et al., 2018. The paradox of irrigation efficiency. Science 361, 748–750. doi:10.1126/science.aat9314.

Hellegers, P., Van Halsema, G., 2021. Sdg indicator 6.4.1 "change in water use efficiency over time": Methodological flaws and suggestions for improvement. Science of The Total Environment 801, 149431. doi:10.1016/j.scitotenv.2021.149431.

Hijmans, R.J., 2025. terra: Spatial Data Analysis. URL: https://CRAN.R-project.org/package=terra, doi:10.32614/CRAN.package.terra. r package version 1.8-54.

Hobbins, M.T., Wood, A., McEvoy, D.J., Huntington, J.L., Morton, C., Anderson, M., Hain, C., 2016. The evaporative demand drought index. part i: Linking drought evolution to variations in evaporative demand. Journal of Hydrometeorology 17, 1745–1761. doi:10.1175/JHM-D-15-0121.1.

Hoekstra, A., Mekonnen, M., 2012. The water footprint of humanity. Proceedings of the National Academy of Sciences 109, 3232–3237. doi:10.1073/pnas.1109936109.

Howden, S., Soussana, J.F., Tubiello, F., Chhetri, N., Dunlop, M., Meinke, H., 2007. Adapting agriculture to climate change. Proceedings of the National Academy of Sciences 104, 19691–19696. doi:10.1073/pnas.0701890104.

Hu, G., Jia, L., 2015. Monitoring of Evapotranspiration in a Semi-Arid Inland River Basin by Combining Microwave and Optical Remote Sensing Observations. Remote Sensing 7, 3056–3087. URL: https://www.mdpi.com/2072-4292/7/3/3056, doi:10.3390/rs70303056.

Immerzeel, W.W., Lutz, A.F., Andrade, M., Bahl, A., Biemans, H., Bolch, T., Hyde, S., Brumby, S., Davies, B.J., Elmore, A.C., et al., 2020. Importance and vulnerability of the world's water towers. Nature 577, 364–369. doi:10.1038/s41586-019-1822-y.

INE, 2007. VII Censo nacional agropecuario y forestal. Instituto Nacional de Estadística. Informe Agropecuarias 2007. Technical Report.

INE, 2021. VIII Censo Nacional Agropecuario y Forestal. Instituto Nacional de Estadísticas. Santiago, Chile. URL: https://www.ine.gob.cl/estadisticas-por-tema/agricultura-y-medio-ambiente/censo-agropecuario. resultados finales publicados en octubre de 2022.

Ito, A., Inatomi, M., 2012. Water-use efficiency of the terrestrial biosphere: A model analysis focusing on interactions between the global carbon and water cycles. Journal of Hydrometeorology 13, 681–694. doi:10.1175/JHM-D-10-05034.1.

Jiang, M., Zheng, C., Jia, L., Chen, J., 2025. A 20-year dataset (2001–2020) of global cropland water-use efficiency at 1-km grid resolution. Scientific Data 12, 574. doi:10.1038/s41597-025-04904-1.

Keenan, T.F., Hollinger, D.Y., Bohrer, G., Dragoni, D., Munger, J.W., Schmid, H.P., Richardson, A.D., 2013. Increase in forest water-use efficiency as atmospheric carbon dioxide concentrations rise. Nature 499, 324–327. URL: https://www.nature.com/articles/nature12291, doi:10.1038/nature12291.

Lutz, A.F., Immerzeel, W.W., Shrestha, A.B., Bierkens, M.F., 2014. Consistent increase in High Asia's runoff due to increasing glacier melt and precipitation. Nature Climate Change 4, 587–592. doi:10.1038/nclimate2237.

Malagueño, B.R., D'Odorico, P., 2024. ¿libre de la maleza estatista? Assessing neoliberal promises and water markets in Chile. Earth's Future doi:10.1029/2024EF004963.

McEvoy, D.J., Huntington, J.L., Hobbins, M.T., Wood, A., Morton, C., Anderson, M., Hain, C., 2016. The evaporative demand drought index. part ii: Conus-wide assessment against common drought indicators. Journal of Hydrometeorology 17, 1763–1779. doi:10.1175/JHM-D-15-0122.1.

Mckee, T.B., Doesken, N.J., Kleist, J., 1993. The relationship of drought frequency and duration to time scales, in: Proceedings of the Ninth Conference on Applied Climatology, American Metereological Society, Boston. pp. 179–184.

Medlyn, B.E., Duursma, R.A., Eamus, D., Ellsworth, D.S., Prentice, I.C., Barton, C.V.M., Crous, K.Y., De Angelis, P., Freeman, M., Wingate, L., 2011. Reconciling the optimal and empirical approaches to modelling stomatal conductance: RECONCILING OPTIMAL AND EMPIRICAL STOMATAL MODELS. Global Change Biology 17, 2134–2144. URL: https://onlinelibrary.wiley.com/doi/10.1111/j.1365-2486.2010.02375.x, doi:10.1111/j.1365-2486.2010.02375.x.

Paruelo, J.M., Texeira, M., Staiano, L., Mastrángelo, M., Amdan, L., Gallego, F., 2016. An integrative index of ecosystem services provision based on remotely sensed data. Ecological Indicators 71, 145–154. doi:10.1016/j.ecolind.2016.06.054.

Patakamuri, S.K., O'Brien, N., 2021. modifiedmk: Modified Versions of Mann Kendall and Spearman's Rho Trend Tests. URL: https://CRAN.R-project.org/package=modifiedmk, doi:10.32614/CRAN.package.modifiedmk. r package version 1.6.

Pebesma, E., 2018. Simple Features for R: Standardized Support for Spatial Vector Data. The R Journal 10, 439–446. URL: https://doi.org/10.32614/RJ-2018-009, doi:10.32614/RJ-2018-009.

Pebesma, E., Bivand, R., 2023. Spatial Data Science: With applications in R. Chapman and Hall/CRC. URL: https://r-spatial.org/book/, doi:10.1201/9780429459016.

Pedersen, T.L., 2025. patchwork: The Composer of Plots. URL: https://CRAN.R-project.org/package=patchwork, doi:10.32614/CRAN.package.patchwork. r package version 1.3.1.

Pettitt, A.N., 1979. A non-parametric approach to the change-point problem. Journal of the Royal Statistical Society: Series C (Applied Statistics) 28, 126–135. doi:10.2307/2346729.

Pohlert, T., 2023. trend: Non-Parametric Trend Tests and Change-Point Detection. URL: https://CRAN.R-project.org/package=trend, doi:10.32614/CRAN.package.trend. r package version 1.1.6.

R Core Team, 2025. R: A Language and Environment for Statistical Computing. R Foundation for Statistical Computing. Vienna, Austria. URL: https://www.R-project.org/.

Rivera, D., Godoy-Faúndez, A., Lillo, M., Alvez, A., Delgado, V., Gonzalo-Martín, C., Menasalvas, E., Costumero, R., García-Pedrero, Á., 2016. Legal disputes as a proxy for regional conflicts over water rights in chile. Journal of Hydrology 535, 36–45. doi:10.1016/j.jhydrol.2016.01.057.

Running, S., Mu, Q., Zhao, M., Moreno, A., 2021. MODIS/Terra net evapotranspiration Gap-Filled 8-day L4 global 500m SIN grid V061.

Sinclair, T.R., 1998. Historical Changes in Harvest Index and Crop Nitrogen Accumulation. Crop Science 38, 638–643. URL: https://acsess.onlinelibrary.wiley.com/doi/10.2135/cropsci1998.0011183X003800030002x, doi:10.2135/cropsci1998.0011183X003800030002x.

Stanhill, G., 1986. Water Use Efficiency, in: Advances in Agronomy. Elsevier. volume 39, pp. 53–85. URL: https://linkinghub.elsevier.com/retrieve/pii/S0065211308604654, doi:10.1016/S0065-2113(08)60465-4.

Tahasin, A., Haydar, M., Hossen, M.S., Sadia, H., 2024. Drought vulnerability assessment and its impact on crop production and livelihood of people: An empirical analysis of Barind Tract. Heliyon 10, e39067. URL: https://linkinghub.elsevier.com/retrieve/pii/S2405844024150980, doi:10.1016/j.heliyon.2024.e39067.

Tennekes, M., 2018. tmap: Thematic maps in R. Journal of Statistical Software 84, 1–39. doi:10.18637/jss.v084.i06.

Vicente-Serrano, S.M., Beguería, S., López-Moreno, J.I., 2010. A multiscalar drought index sensitive to global warming: The standardized precipitation evapotranspiration index. Journal of Climate 23, 1696–1718. doi:10.1175/2009JCLI2909.1.

Wallace, J., 2000. Increasing agricultural water use efficiency to meet future food production. Agriculture, Ecosystems & Environment 82, 105–119. URL: http://dx.doi.org/10.1016/S0167-8809(00)00220-6, doi:10.1016/s0167-8809(00)00220-6.

Wang, T., Sun, S., Yin, Y., Zhao, J., Tang, Y., Wang, Y., Gao, F., Luan, X., 2024. Status of crop water use efficiency evaluation methods: A review. Agricultural and Forest Meteorology 349, 109961. doi:10.1016/j.agrformet.2024.109961.

Ward, F.A., Pulido-Velázquez, M., 2008. Water conservation in irrigation can increase water use. Proceedings of the National Academy of Sciences 105, 18215–18220. doi:10.1073/pnas.0805554105.

Wickham, H., 2016. ggplot2: Elegant Graphics for Data Analysis. Springer-Verlag New York. URL: https://ggplot2.tidyverse.org.

Wickham, H., Averick, M., Bryan, J., Chang, W., McGowan, L.D., François, R., Grolemund, G., Hayes, A., Henry, L., Hester, J., Kuhn, M., Pedersen, T.L., Miller, E., Bache, S.M., Müller, K., Ooms, J., Robinson, D., Seidel, D.P., Spinu, V., Takahashi, K., Vaughan, D., Wilke, C., Woo, K., Yutani, H., 2019. Welcome to the tidyverse. Journal of Open Source Software 4, 1686. doi:10.21105/joss.01686.

Xie, W., Zhu, A., Ali, T., Zhang, Z., Chen, X., Wu, F., Huang, J., Davis, K., 2023. Crop switching can enhance environmental sustainability and farmer incomes in china. Nature 616, 300–305. doi:10.1038/s41586-023-05799-x.

Yu, L., Gao, X., Zhao, X., 2020. Global synthesis of the impact of droughts on crops' water-use efficiency (WUE): Towards both high WUE and productivity. Agricultural Systems 177, 102723. URL: https://linkinghub.elsevier.com/retrieve/pii/S0308521X19301568, doi:10.1016/j.agsy.2019.102723.

Yu, X., Yin, Q., Zhao, T., Chen, K., Qian, L., Wang, W., Hu, X., Zhang, B., 2025. Detecting ecosystem water use efficiency responses to drought from long-term remote sensing data. Ecological Indicators 177, 113734. URL: https://linkinghub.elsevier.com/retrieve/pii/S1470160X25006648, doi:10.1016/j.ecolind.2025.113734.

Zambrano, F., Vrieling, A., Meza, F., Duran-Llacer, I., Fernández, F., Venegas-González, A., Raab, N., Craven, D., 2025. From Drought to Aridification: Land-Cover Fingerprints of a Drying Chile. Earth's Future 13, e2025EF006744. URL: https://agupubs.onlinelibrary.wiley.com/doi/10.1029/2025EF006744, doi:10.1029/2025EF006744.

Zwart, S.J., Bastiaanssen, W.G., 2004. Review of measured crop water productivity values for irrigated wheat, rice, cotton and maize. Agricultural Water Management 69, 115–133. URL: https://linkinghub.elsevier.com/retrieve/pii/S0378377404001416, doi:10.1016/j.agwat.2004.04.007.